NeuroImage 187 (2019) 176–183

Contents lists available at ScienceDirect

NeuroImage

journal homepage: www.elsevier.com/locate/neuroimage

MR elastography of the brain and its application in neurological diseases

Matthew C. Murphy *, John Huston III, Richard L. Ehman

Department of Radiology, Mayo Clinic, Rochester, MN, United States

A B S T R A C T

Magnetic resonance elastography (MRE) is an imaging technique for noninvasively and quantitatively assessing tissue stiffness, akin to palpation. MRE is further able assess the mechanical properties of tissues that cannot be reached by hand including the brain. The technique is a three-step process beginning with the introduction of shear waves into the tissue of interest by applying an external vibration. Next, the resulting motion is imaged using a phase-contrast MR pulse sequence with motion encoding gradients that are synchronized to the vibration. Finally, the measured displacement images are mathematically inverted to compute a map of the estimated stiffness. In the brain, the technique has demonstrated strong test-retest repeatability with typical errors of 1% for measuring global stiffness, 2% for measuring stiffness in the lobes of the brain, and 3–7% for measuring stiffness in subcortical gray matter. In healthy volunteers, multiple studies have confirmed that stiffness decreases with age, while more recent studies have demonstrated a strong relationship between viscoelasticity and behavioral performance. Furthermore, several studies have demonstrated the sensitivity of brain stiffness to neurodegeneration, as stiffness has been shown to decrease in multiple sclerosis and in several forms of dementia. Moreover, the spatial pattern of stiffness changes varies among these different classes of dementia. Finally, MRE is a promising tool for the preoperative assessment of intracranial tumors, as it can measure both tumor consistency and adherence to surrounding tissues. These factors are important predictors of surgical difficulty. In brief, MRE demonstrates potential value in a number of neurological diseases. However, significant opportunity remains to further refine the technique and better understand the underlying physiology.

The mechanical properties of tissues have long been assessed qualitatively in the practice of medicine by palpation, as tissues throughout the body have stiffness that span several orders of magnitude and alterations in tissue stiffness are known to coincide with pathological processes. Magnetic resonance elastography (MRE) is an MR-based technique for noninvasively measuring tissue stiffness (Muthupillai et al., 1995). This technique offers benefits beyond traditional palpation by providing a quantitative assessment, which allows for objective disease staging and monitoring, as well as enabling measurement of mechanical properties in tissues that cannot be reached by hand, such as the brain.

Performance of MRE follows a three-step process. First, shear waves are introduced into the tissue of interest by applying an external vibration. Second, the resulting displacement is measured using a phase-contrast MRI pulse sequence by applying motion encoding gradients that are synchronized to the vibration. Third, an inversion algorithm is used to estimate stiffness from the measured displacement field. Each of these steps is further discussed below, with particular emphasis on implementations typically used in the brain, as well as an overview of the state-of-the-art in measuring stiffness *in vivo* in both health and disease. While we present an overview of the MRE method here, a thorough review of all methodologies used in the brain MRE literature can be found in (Hiscox et al., 2016).

Shear wave generation

Most MRE studies are performed using harmonic motion, in which vibration is applied at a prescribed frequency of interest until a steady state has been reached before imaging the resulting displacement field. The earliest brain MRE studies introduced intracranial shear waves by electromechanical actuators that were attached either to a cradle below the subject's head or to a subject-specific bite bar (Green et al., 2008; Kruse et al., 2008). More recently, pneumatic systems have become more popular, where a speaker system (sometimes referred to as an active driver) produces sinusoidal displacements of the desired frequency that are transmitted to the subject's head either by a passive, pillow-like driver (Murphy et al., 2011), or by a head-rocker via a rigid rod (Klatt et al., 2007). The choice of vibrational frequency is application dependent, with the optimal signal-to-noise ratio (SNR) determined by the tradeoff between two competing effects. On the one hand, higher frequency vibrations have shorter wavelengths. As stiffness estimation relies on calculation of spatial derivatives, for a given wave amplitude, shorter wavelengths will have larger spatial derivatives and thus greater SNR. On the other hand, the viscous behavior of soft biological tissues results in attenuation of motion amplitude as a wave moves away from its source, with higher frequency waves tending to attenuate more quickly than lower frequency waves. When characterizing mechanical properties

* Corresponding author. Department of Radiology, Mayo Clinic, 333 Fourth Ave SW, Rochester, MN 55902, United States.
E-mail address: murphy.matthew@mayo.edu (M.C. Murphy).

https://doi.org/10.1016/j.neuroimage.2017.10.008
Received 1 August 2017; Received in revised form 4 October 2017; Accepted 5 October 2017
Available online 7 October 2017

throughout the entire brain, our group most often applies vibration at 60 Hz (Murphy et al., 2013b), as our experience is this is the highest frequency we can apply while still achieving adequate displacement amplitude in deep structures in the majority of subjects. Most work in the brain is performed in the range of 25–62.5 Hz (Hatt et al., 2015; Johnson et al., 2016; Murphy et al., 2013b; Sack et al., 2009), while some approaches utilize multiple frequencies in this range to further model viscoelastic properties as a function of frequency (Dittmann et al., 2016; Guo et al., 2013; Sack et al., 2009).

MRE acquisition strategies

MR pulse sequences can be modified for MRE by the addition of a motion encoding gradient (MEG). The integral of this gradient waveform is 0, thus not altering the position of sampling in the frequency domain, but the phase of the signal is modulated in a way that is proportional to the dot product of the MEG and the applied motion:

$$\varphi = \gamma \int_0^{\tau} MEG(t) \cdot r(t) dt$$

Here, φ is the phase of the MR signal, γ is the gyromagnetic ratio, MEG is the motion encoding gradient waveform, and r is the position of the spins. Intuitively, as the spins move up the magnetic gradient, the frequency of precession is increased, and a certain phase is accrued. If when those spins reverse course, the polarity of the motion encoding gradient is simultaneously flipped, then again the spins will move up the magnetic gradient and accrue additional phase. In this way, the gradient encodes the amplitude of motion in the phase of the MR image.

With respect to MRE of the brain, most applications now take advantage of rapid acquisition schemes that acquire a plane of k-space per repetition, such as echo-planar imaging (EPI) (Klatt et al., 2007; Murphy et al., 2011), spiral imaging (Johnson et al., 2013b), or more recently a 3D multislab strategy (Johnson et al., 2014). Given the widespread use of EPI pulse sequences in many neuroimaging applications, these data can be reconstructed on the host system, which should aid future clinical implementation. On the other hand, Non-Cartesian pulse sequences often require off-line reconstruction but provide convenient methods to include navigators (to correct motion-induced phase errors), and in the case of the multislab acquisition, can shorten the repetition time to improve SNR efficiency. These acquisition strategies each allow volumetric coverage with the repeated sampling necessary for MRE, while still maintaining a well-tolerated acquisition time. Repeated sampling of the full volume is necessary for two reasons. First, due to the complex displacement field in the brain, the x, y and z components of the displacement field must each be measured. Typically, a given direction of motion is estimated by applying a MEG in both the positive and negative direction, and taking the difference in phase measured by these two acquisitions. In this way, the motion sensitivity is doubled, and artifacts due to static background phase are reduced. This motion encoding scheme would thus require 6 measurements. Faster motion encoding schemes are available at the expense of SNR (Klatt et al., 2015). Second, to estimate the harmonic motion at the frequency of interest, multiple measurements of the displacement field across the period of motion are necessary, which is achieved by placing a phase offset between the applied motion and the start of the MR acquisition. A common choice throughout the field of MRE is 4 samples spaced evenly over one period of the motion.

Stiffness estimation

In the most basic sense, shear waves will propagate more quickly through a stiff material (corresponding to a longer wavelength) than through a softer material (shorter wavelength). Given that the brain exhibits viscoelastic behavior, its shear mechanical properties are expressed as a complex modulus with a real part (or storage modulus) that reflects the elastic behavior of the material, and an imaginary part (or loss modulus) that is related to energy loss due to either absorption or scattering. Stiffness estimates determined by MRE reflect the effective, macroscopic properties of the tissue at a scale on the order of the wavelength, and are influenced by the mechanical properties of the underlying cells and extracellular matrix, as well as the interaction between these components. It has been suggested that neuronal properties are particularly important in determining the brain's elasticity, while quantities more closely related to the loss modulus reflect the underlying cellular architecture or geometry perhaps across multiple spatial scales (Freimann et al., 2013; Hain et al., 2016; Johnson et al., 2013a; Klein et al., 2014; Streitberger et al., 2012). These interpretations with respect to the effects scattering and geometry on the loss modulus are supported by simulation and phantom experiments (Guo et al., 2012; Juge et al., 2015; Lambert et al., 2015; Posnansky et al., 2012), but still require validation *in vivo*.

Several classes of algorithms exist for quantitatively estimating stiffness given a measured displacement field; however the most commonly used algorithms in the brain are currently either some form of direct inversion (Hirsch et al., 2014; Oliphant et al., 2001; Papazoglou et al., 2008) or non-linear inversion (McGarry et al., 2012; Van Houten et al., 2001; Van Houten et al., 1999). Both the direct inversion and non-linear inversion algorithms estimate this complex shear modulus, from which a number of other quantities of interest can be calculated such as wave speed or damping ratio. Direct inversion algorithms solve the equations of wave motion in a viscoelastic material. Typically these inversions are simplified by a number of assumptions including linear and isotropic elasticity and local tissue homogeneity (Hirsch et al., 2014; Oliphant

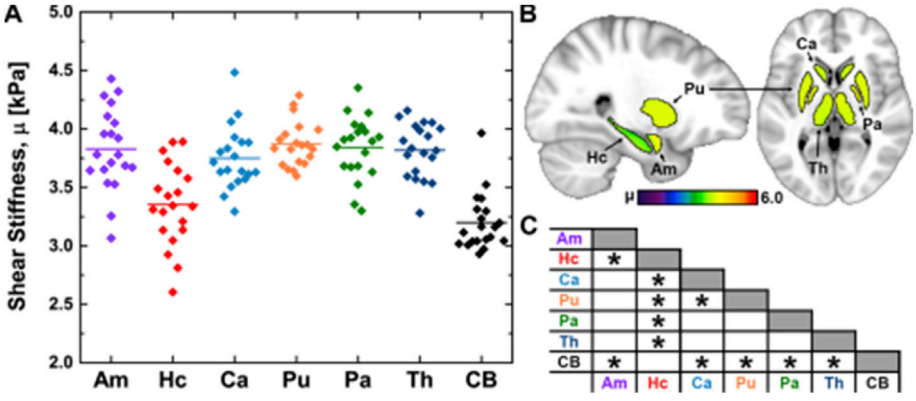

Fig. 1. (Johnson et al., 2016). Summary of shear stiffness in subcortical gray matter structures including amygdala (Am), hippocampus (Hc), caudate (Ca), putamen (Pu), palldium (pa), and thalamus (Th). Surrounding cerebrum (CB) is also included for reference. A. Plot presents the mean stiffness for each participant by region with the line indicating the group mean. B. Image shows the mean shear stiffness of each structure after normalization to a common space. C. Table summarizes pair-wise comparisons of stiffness between regions as assessed by paired t-tests (*p < 0.05 with Bonferroni correction).

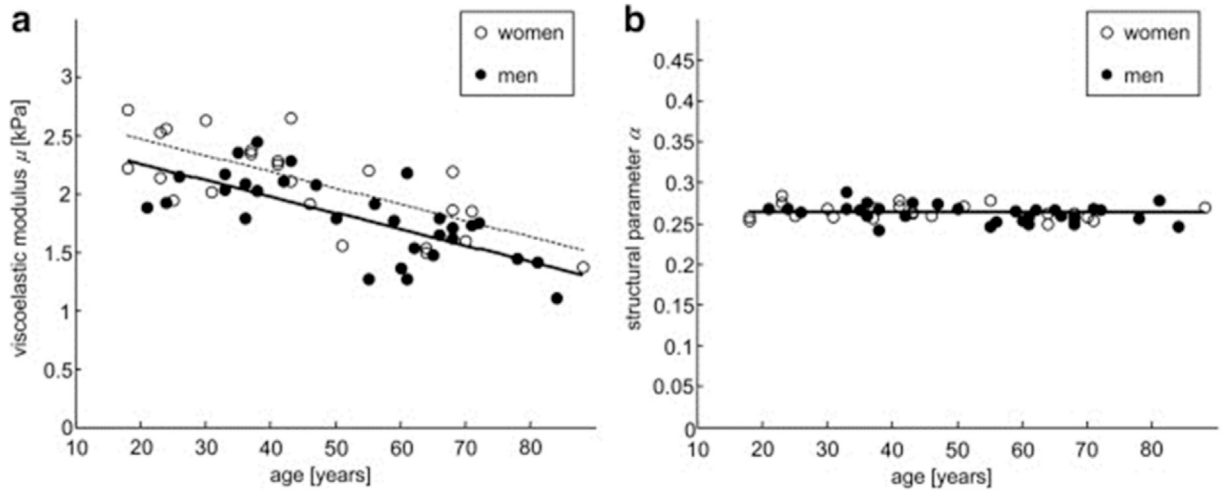

Fig. 2. (Sack et al., 2009). Summary of the relationship between global brain viscoelasticity and age. Stiffness estimates over multiple frequencies were fit to a two-parameter springpot model. a. The viscoelastic modulus from this model (μ) decreases significantly with age and is larger in women compared to men. b. The structural parameter (α) displays no significant effects due to age or sex.

et al., 2001; Papazoglou et al., 2008). Since these methods require the estimation of spatial derivatives of the displacement field (at least second order and up to third order derivatives depending on implementation), the resulting stiffness estimates can be noisy in practice, often requiring some combination of filtering, or the use of multiple displacement fields (Hirsch et al., 2014), to stabilize the results. Non-linear inversion utilizes an iterative approach to estimate the complex shear modulus by minimizing error between the measured displacement and a simulated displacement field based on a finite element model, which is parameterized by the stiffness estimate (Van Houten et al., 2001; Van Houten et al., 1999). This inversion is run on overlapping subzones of the displacement field, with these results then combined to compute the full stiffness map. A major advantage of non-linear inversion is that it relaxes the assumption of local tissue homogeneity. However, the algorithm can require several hours to run and is sensitive to tuning parameters.

Stiffness measurements in healthy volunteers

Now that the field of brain MRE has agreed on some common principles, notably including three-dimensional analysis of the displacement field for stiffness estimation and accounting for noise and partial volume effects, brain stiffness can be reliably measured both globally and regionally. Stiffness estimates, however, are sensitive to experimental choices including vibrational frequency, acquisition strategy, and processing pipelines. Therefore, it has proven challenging to quantitatively assess reproducibility of stiffness estimates across sites, and it is important that these parameters are held constant when making any inferences about the effects of biological processes on stiffness. Using our current acquisition and processing pipeline, we have shown test-retest repeatability with typical errors of 1% for measuring global stiffness, and 2% for measuring stiffness in the lobes of the brain (Murphy et al., 2013b). Johnson et al. have focused their acquisition more directly on measuring stiffness in subcortical gray matter, which is summarized in Fig. 1, and report repeatability in the range of 3–7% in these smaller regions (Johnson et al., 2016). Both of these methods agree that deep gray nuclei are stiffer than surrounding white matter; however the mean shear modulus map shown by Guo et al. appears to show relatively lower stiffness in these regions (Guo et al., 2013). There is also agreement that stiffness in the cerebellum is lower than that observed in the cerebrum (Murphy et al., 2013b; Zhang et al., 2011).

A number of studies on healthy aging have now been completed, and a consensus has formed that brain stiffness decreases with age (Arani et al., 2015; Sack et al., 2009, 2011). A summary from the earliest of these studies by Sack et al. is included in Fig. 2. The effect of sex is more equivocal with this initial study by Sack et al. exhibiting higher global stiffness in female subjects (Sack et al., 2009), while a later study did not detect a significant effect (Sack et al., 2011). More recently, a study by our group indicated that a sex-effect on stiffness was only significant in the occipital and temporal lobes (Arani et al., 2015). The regional dependence of this effect may therefore help explain the earlier discrepancies.

An intriguing new direction in brain MRE research is the use of stiffness to study the relationship between structure and function in the healthy brain. Schwarb et al. have performed pioneering work in this area, demonstrating that damping ratio in the hippocampus (essentially how quickly shear waves attenuate) is a significant predictor of performance on a relational memory task (Fig. 3). Even more intriguingly, damping ratio was able to predict this behavioral performance while no

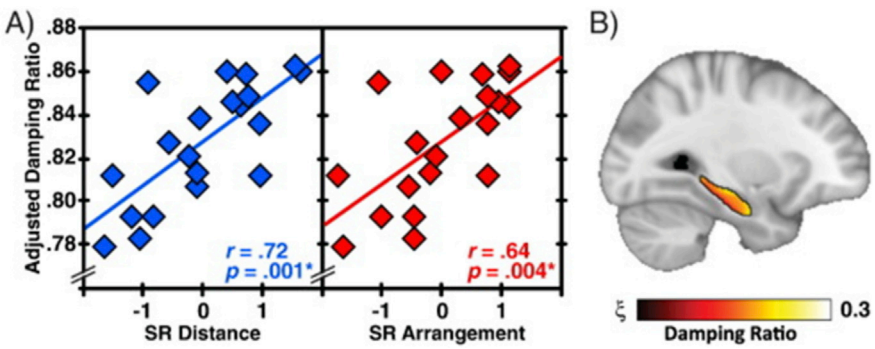

Fig. 3. (Schwarb et al., 2016). Summary of relationship between hippocampal damping ratio and performance on a spatial reconstruction (SR) task. A. Scatter plots of adjusted damping ratio versus performance as measured by either the total distance of object misplacement (SR Distance) or by the number of arrangement errors (SR Arrangement). Performance metrics were normalized and adjusted so that larger scores reflect better performance. B. This image displays the average damping ratio across all subjects in a common space.

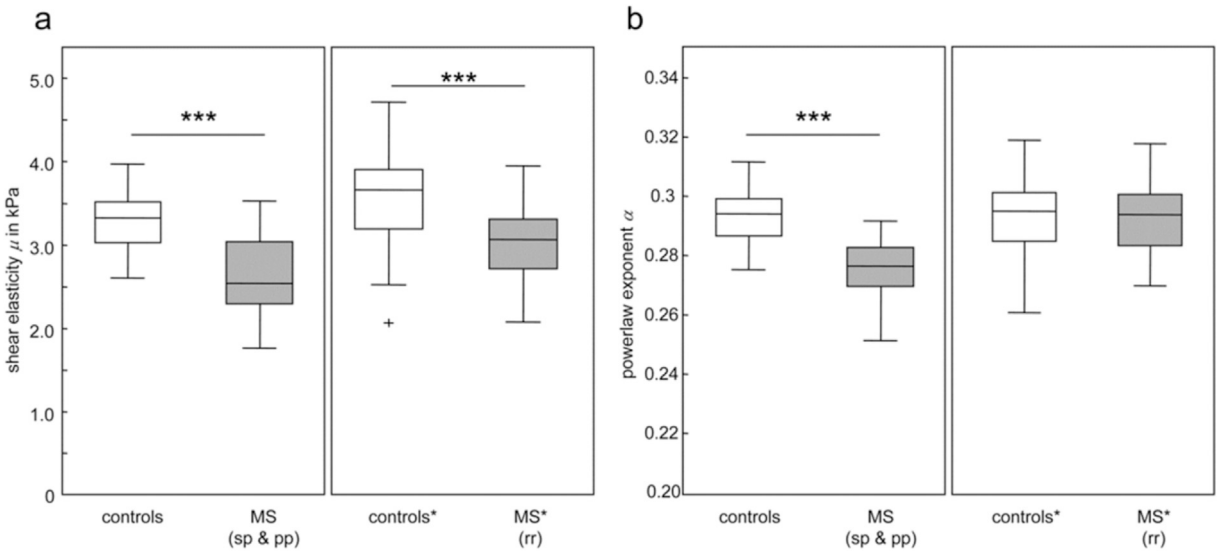

Fig. 4. (Streitberger et al., 2012). Summary of viscoelasticity in subjects with multiple sclerosis (MS) compared to age-matched controls. Stiffness estimates over multiple frequencies were fit to a two-parameter springpot model. a. Shear elasticity (μ) was reduced in MS patients with a secondary (sp) or primary (pp) chronic progressive course, as well as in patients with a relapsing-remitting (rr) disease course. b. The powerlaw exponent (or structural parameter, α) was only reduced in the chronic progressive disease course.

relationship could be observed with hippocampal volume in this group of young adults (Schwarb et al., 2016). This result was replicated in a follow up study, which also showed a relationship between aerobic fitness and hippocampal viscoelasticity (Schwarb et al., 2017). Taken together, their studies provide strong evidence for viscoelasticity as a highly sensitive correlate of tissue function.

Another active area of research in brain MRE relates to the effect of anisotropy on stiffness estimates. While most applications of brain MRE assume an isotropic material (in order to make stiffness estimation from the vector components of the displacement field separable), we know this assumption does not hold in the brain. Myelinated white matter tracts contain highly organized axons that are ensheathed and bound together by oligodendrocytes. One would expect this organization to impact the bulk mechanical properties as a function of fiber orientation, as has been observed in muscle where shear waves propagate more quickly along the direction of the fibers (Gennisson et al., 2003, 2010; Kruse et al., 2000; Papazoglou et al., 2006). To attempt to measure this anisotropic effect, Romano et al. have proposed an inversion algorithm that measures stiffness both parallel and perpendicular to the fiber orientation leveraging diffusion imaging to define the fiber coordinate system at each voxel (Romano et al., 2012). Tweten et al. also developed a method to assess stiffness in a transversely isotropic material using directional filtering, while also establishing criteria that must hold for valid parameter estimation and evaluating the technique in a set of finite element simulations (Tweten et al., 2015, 2017). Schmidt et al. then applied this theory demonstrating that the expected fast and slow shear waves can be detected both in phantom and in *ex vivo* specimens of muscle (Schmidt et al., 2016). In a human study, Anderson et al. observed that stiffness estimates were altered by changing the primary direction of vibration, presumably attributable to the anisotropy of the white matter

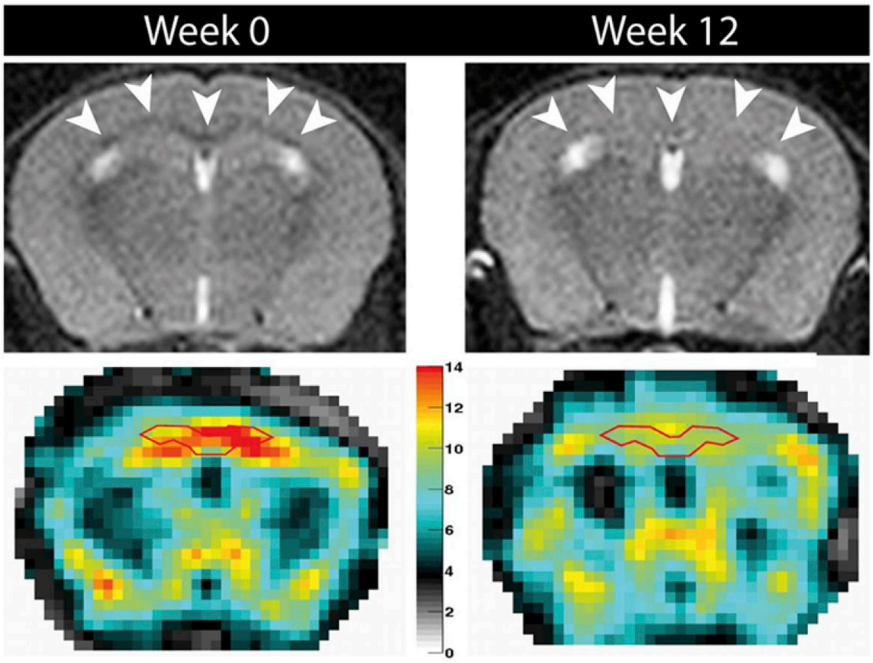

Fig. 5. (Schregel et al., 2012). Example images from a control mouse (left) and a mouse undergoing 12 weeks of cuprizone diet (right). In the control mouse, the corpus callosum is easily identified in the T2-weighted anatomical image (top, white arrows) and observed to be relatively firm in the corresponding stiffness map (bottom, red outline). In the experimental animal, the corpus callosum is not apparent on T2-weighted imaging and the stiffness is markedly reduced.

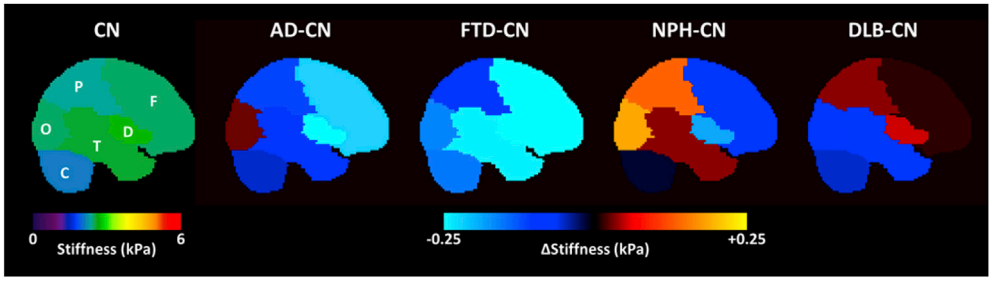

Fig. 6. (data from ElSheikh et al., 2017). Summary of stiffness changes due to 4 forms of dementia. In the first panel is a sagittal view of a lobar brain atlas with each region showing the mean stiffness in a group of cognitively normal (CN) control subjects. Regions include frontal lobe (F), parietal lobe (P), temporal lobe (T), occipital lobe (O), deep gray and white matter (D), and cerebellum (C). The remaining panels display the difference between mean stiffness in the dementia group and the CN group. These 4 groups include Alzheimer's disease (AD), frontotemporal dementia (FTD), normal pressure hydrocephalus (NPH), and dementia with Lewy bodies (DLB).

(Anderson et al., 2016). While further work is needed to accurately characterize anisotropy of mechanical properties in the brain, a study by Romano et al. in amyotrophic lateral sclerosis has shown evidence that certain components of the anisotropic shear modulus are more sensitive to degeneration in the corticospinal tract, supporting the need for further investigation into anisotropic reconstructions (Romano et al., 2014).

Brain stiffness is sensitive to demyelination

The first demonstration of the sensitivity of brain stiffness to pathology was presented by Wuerfel et al. in a study of multiple sclerosis (MS). This work showed that global stiffness was decreased in subjects with MS compared to age-matched control subjects (Wuerfel et al., 2010). The effect of disease course was then evaluated by Streitberger et al. In this study, multi-frequency data were fit to a two-parameter viscoelastic model, known as the springpot model, which provides an estimate of the shear elasticity and a powerlaw exponent. The study concluded that while elasticity was reduced by both the relapsing-remitting and chronic-progressive disease courses, only the chronic-progressive course caused a reduction in the powerlaw exponent (Fig. 4). This latter finding was interpreted as altered cerebral geometry, which was unique to the chronic form of the disease (Streitberger et al., 2012).

The sensitivity of brain stiffness to demyelination is well-supported in animal models of MS. Schregel et al. induced demyelination in a mouse model by introduction of cuprizone into the animals' diet. In comparing stiffness measurements with histology, they found that the magnitude of the complex shear modulus was decreased with demyelination and breakdown of the extracellular matrix. Example images demonstrating this effect are shown in Fig. 5. Also, by removing cuprizone to reverse demyelination, they showed that the mechanical properties of the tissue were restored, lending further evidence to a causal relationship between demyelination and decreased brain stiffness (Schregel et al., 2012). Somewhat similarly, Riek et al. observed decreased storage and loss moduli in a relapsing-remitting experimental autoimmune encephalomyelitis (EAE) mouse model in the first two weeks following induction, which then recovered as inflammation was reduced over the following two weeks. Overall, they concluded that brain stiffness was correlated with T cell infiltration as assessed by CD3 immunostaining (Riek et al., 2012). The effect of a chronic EAE model on viscoelasticity was somewhat different, as no changes in cerebral mechanical properties were observed in C57Bl/6 mice. However, when the phenotype was exacerbated in a mouse line that lacks the cytokine, interferon-gamma, again a correlation was observed between change in stiffness and macrophage/microglia infiltration as assessed by F4/80 gene expression (Millward et al., 2015).

Brain stiffness as a biomarker of dementia

One major focus of our lab has been the investigation of brain stiffness as a biomarker for dementias. In our first human study, we showed that global brain stiffness was decreased in subjects with Alzheimer's disease (AD), but that amyloid deposition alone was insufficient to cause a change in stiffness (Murphy et al., 2011). This reduction in stiffness may reflect a number of microstructural events that characterize AD including degradation of the extracellular matrix (due to amyloid deposition), loss of normal cytoskeletal architecture (due to Tau hyper-phosphorylation), or altered synaptic connectivity. We followed this study with a regional investigation of brain stiffness in AD. The study confirmed that global stiffness was diminished in subjects with AD, but further demonstrated the specificity of stiffness changes, as the decreases were observed in heteromodal association cortices that are hardest hit by the disease but not throughout the rest of the brain. Brain stiffness was further shown to correlate with disease severity as assessed by established AD biomarkers including PIB PET imaging (to assess amyloid deposition), hippocampal volume, and even to functional connectivity within the default mode network (Murphy et al., 2016). The sensitivity of brain stiffness to AD pathophysiology is further supported by animal studies, which show that stiffness is altered in mouse models of the disease (Munder et al., 2017; Murphy et al., 2012). Also related, mouse models of both stroke (Freimann et al., 2013) and Parkinson's disease (Hain et al., 2016; Klein et al., 2014) have demonstrated a significant relationship between viscoelasticity and neuronal density, which could explain the findings in humans. However, interpretation of these animal studies is complicated by confounding physiological processes including inflammation, edema, and neovascularization.

The regional specificity of brain stiffness as a biomarker of dementia is further supported by work from our group and others. Stiffness changes associated with four classes of dementia have recently been summarized by ElSheikh et al., and are summarized schematically in Fig. 6 (ElSheikh et al., 2017). While AD was shown to impact the frontal, parietal and temporal lobes (Murphy et al., 2016), frontotemporal dementia showed only significantly decreased stiffness in the frontal and temporal lobes (Huston et al., 2016). Preliminary evidence in dementia with Lewy bodies indicated no evidence of stiffness changes relative to age-matched controls (ElSheikh et al., 2017). Finally, our group has reported increased stiffness in the parietal and occipital lobes in patients with normal pressure hydrocephalus (NPH) (Perry et al., 2017). However, this finding does not agree with previous work from Friemann et al. and Streitberger et al., which reported decreased global stiffness in NPH (Freimann et al., 2012; Streitberger et al., 2011). Differences may be due to the use of global versus regional measurements and techniques used for dealing with partial volume effects, but further investigation is needed to resolve this discrepancy. Finally, Lipp et al. reported decreased stiffness due to idiopathic Parkinson's disease and progressive supranuclear palsy (PSP). This reduction in brain stiffness was more severe in subjects with PSP, and was strongest in the lentiform nucleus as expected (Lipp et al., 2013).

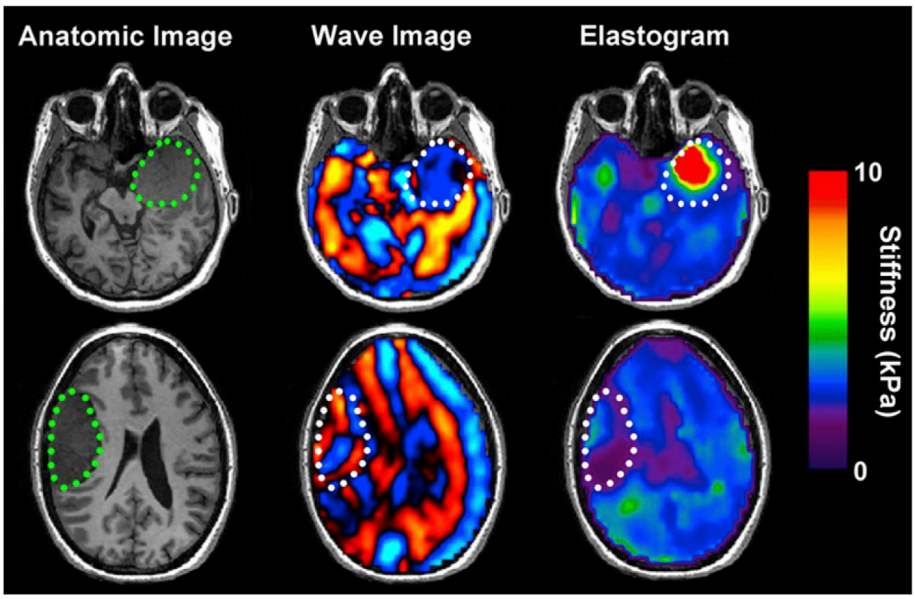

Fig. 7. (Murphy et al., 2013a). Example MRE images from both a firm (top) and soft (bottom) meningioma case. On the left is a T1-weighted anatomical image. Example wave images are shown in the middle column, showing an elongated wavelength in the firm tumor and shortened wavelength in the soft tumor relative to surrounding brain parenchyma. Finally, the resulting stiffness maps are shown in the right column.

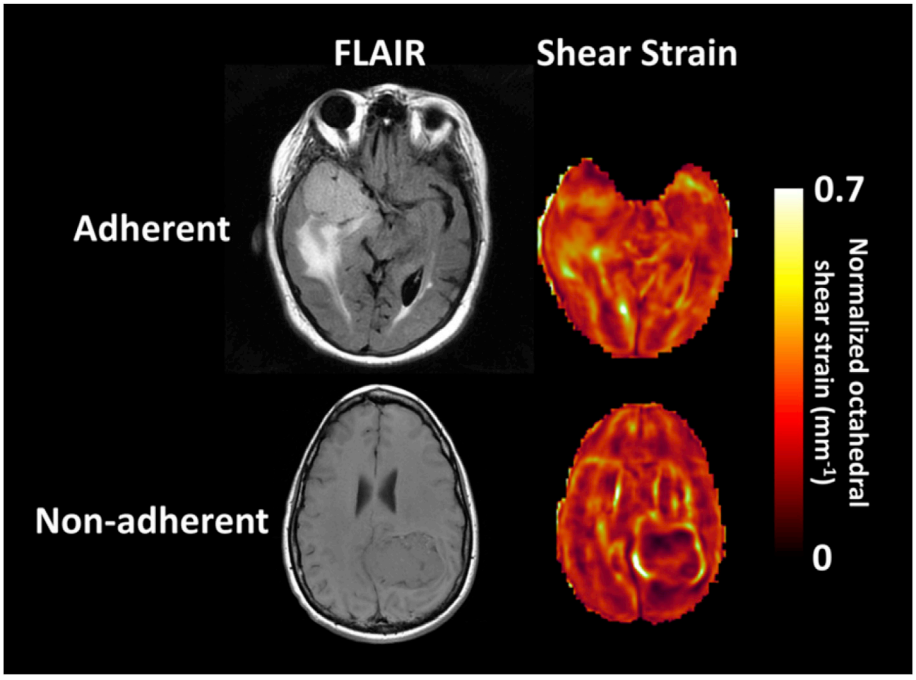

Fig. 8. (data from Yin et al., 2017). Example slip interface images from both an adherent (top) and non-adherent (bottom) meningioma case. The tumor location can be seen in the T2-weighted FLAIR images in the left column. The shear strain maps are shown on the right. Note the bright ring around the tumor in the non-adherent case, which is absent in the adherent case.

MRE for preoperative assessment of intracranial tumors

In intracranial tumors requiring surgery, one of the most important factors determining the difficulty of resection is the consistency of the tumor. Whereas soft tumors can be more easily removed, often by suction, firm tumors are more difficult, often requiring manual dissection. For this reason, preoperative assessment of tumor consistency by imaging has long been the subject of research (Chernov et al., 2011; Hoover et al., 2011; Kashimura et al., 2007; Kendall and Pullicino, 1979; Smith et al., 2016; Suzuki et al., 1994; Yamaguchi et al., 1997). However, MRI alone can only differentiate the stiffest and softest tumors (Hoover et al., 2011). A direct assessment of the tumor mechanical properties would therefore be valuable in this regard. The use of MRE to assess intracranial tumors was first demonstrated by Xu et al., indicating the large variability present in the viscoelasticity of these tumors (Xu et al., 2007). Our group has published two manuscripts on the use of MRE to evaluate meningiomas, indicating that stiffness is correlated with the surgeons' assessment of tumor consistency. However, challenges still remain in small and/or heterogeneous tumors, as well understanding the effects of vascularity on the MRE measurements (Hughes et al., 2015; Murphy et al., 2013a).

Example images from a firm and soft tumor are shown in Fig. 7.

Another important factor in determining the difficulty of resection is the adherence of the tumor to the surrounding tissue, where tumors that are adherent are more difficult to remove. To address this problem, slip interface imaging (SII) was developed and evaluated in both vestibular schwannomas (Yin et al., 2015) and meningiomas (Yin et al., 2017). The basic idea underlying SII is that if two adjacent compartments of tissue are free to move independently of one another, then as a shear wave propagates across the boundary, a discontinuity will be created. This discontinuity can be detected by computing a map of shear strain, which appears large in magnitude at the sites of these discontinuities. This technique has demonstrated a strong prediction of tumor adherence in both types of tumors investigated. Example slip interface images from an adherent and non-adherent meningioma are shown in Fig. 8.

Conclusions and future directions

To date, the field of brain MRE has shown that brain stiffness has great potential to detect biological processes in both health and disease. Stiffness is shown to decrease with age, and hippocampal damping ratio can predict performance on a memory task. Brain stiffness is also sensitive to demyelination and neurodegeneration, with regional specificity to differentiate between forms of dementia. Finally, MRE demonstrates strong potential value in the preoperative assessment of intracranial tumors, including evaluation of both tumor consistency and adhesion.

Still, much work remains to optimize and more accurately interpret MRE in the brain. We feel the areas that require immediate attention fall in two main categories. First, in the area of technical development, further improvements in resolution are necessary. These improvements may come through advances in acquisition strategies, where approaches such as shortened repetition times (Johnson et al., 2014) or higher field strength (Braun et al., 2014) have been suggested to boost SNR at a given resolution, or in stiffness estimation, where investigations are ongoing into nonlinear preprocessing of the displacement data (Barnhill et al., 2017) and the use of multi-frequency data for inversion (Hirsch et al., 2014). While the impact of acquisition on resolution is relatively straightforward, inversions that produce accurate, stable stiffness estimates with a controlled spatial footprint will serve to improve the effective resolution of MRE. Resolution improvements would benefit any application of MRE in the brain. With respect to diffuse processes, we would like to measure stiffness in the cortex, where we expect larger effects due to pathological or physiological changes. With respect to focal diseases such as tumors, low spatial resolution limits the accuracy of stiffness estimates in small regions of interest. To assess smaller tumors, we need more accurate stiffness estimates at the region's edge. Second, more investigation is needed into the biological basis of stiffness and the mechanisms underlying stiffness changes. How is stiffness affected by perfusion (Hetzer et al., 2017), extracellular matrix composition (Schregel et al., 2012), intracranial pressure (Arani et al., 2017; Hatt et al., 2015), inflammation (Fehlner et al., 2016; Riek et al., 2012), pathology (Munder et al., 2017; Murphy et al., 2012, 2011, 2016; Riek et al., 2012; Schregel et al., 2012), cellular organization, and cellular morphology? Can we use other MRI-based biomarkers to help tease apart these effects? While some valuable work has been performed in this area, it is largely limited to observational studies. Further experiments in animal models that can establish causality between these processes and alterations in mechanical properties are still necessary. This knowledge will improve the interpretation of MRE to further explain brain structure and how it is related to function and pathology.

Declaration of interest

The authors and Mayo Clinic have a financial conflict of interest related to research funded by this grant.

Acknowledgements

The authors are supported by the National Institutes of Health grant R37-EB001981.

References

Anderson, A.T., Van Houten, E.E., McGarry, M.D., Paulsen, K.D., Holtrop, J.L., Sutton, B.P., Georgiadis, J.G., Johnson, C.L., 2016. Observation of direction-dependent mechanical properties in the human brain with multi-excitation MR elastography. J. Mech. Behav. Biomed. Mater 59, 538–546.

Arani, A., Min, H.K., Fattahi, N., Wetjen, N.M., Trzasko, J.D., Manduca, A., Jack Jr., C.R., Lee, K.H., Ehman, R.L., Huston 3rd, J., 2017. Acute pressure changes in the brain are correlated with MR elastography stiffness measurements: initial feasibility in an in vivo large animal model. Magn. Reson Med. https://doi.org/10.1002/mrm.26738. Epub ahead of print.

Arani, A., Murphy, M.C., Glaser, K.J., Manduca, A., Lake, D.S., Kruse, S.A., Jack Jr., C.R., Ehman, R.L., Huston 3rd, J., 2015. Measuring the effects of aging and sex on regional brain stiffness with MR elastography in healthy older adults. Neuroimage 111, 59–64.

Barnhill, E., Hollis, L., Sack, I., Braun, J., Hoskins, P.R., Pankaj, P., Brown, C., van Beek, E.J.R., Roberts, N., 2017. Nonlinear multiscale regularisation in MR elastography: towards fine feature mapping. Med. Image Anal. 35, 133–145.

Braun, J., Guo, J., Lutzkendorf, R., Stadler, J., Papazoglou, S., Hirsch, S., Sack, I., Bernarding, J., 2014. High-resolution mechanical imaging of the human brain by three-dimensional multifrequency magnetic resonance elastography at 7T. Neuroimage 90, 308–314.

Chernov, M.F., Kasuya, H., Nakaya, K., Kato, K., Ono, Y., Yoshida, S., Muragaki, Y., Suzuki, T., Iseki, H., Kubo, O., Hori, T., Okada, Y., Takakura, K., 2011. (1)H-MRS of intracranial meningiomas: what it can add to known clinical and MRI predictors of the histopathological and biological characteristics of the tumor? Clin. Neurol. Neurosurg. 113, 202–212.

Dittmann, F., Hirsch, S., Tzschatzsch, H., Guo, J., Braun, J., Sack, I., 2016. In vivo wideband multifrequency MR elastography of the human brain and liver. Magn. Reson Med. 76, 1116–1126.

ElSheikh, M., Arani, A., Perry, A., Boeve, B.F., Meyer, F.B., Savica, R., Ehman, R.L., Huston 3rd, J., 2017. MR elastography demonstrates unique regional brain stiffness patterns in dementias. AJR Am. J. Roentgenol. 1–6.

Fehlner, A., Behrens, J.R., Streitberger, K.J., Papazoglou, S., Braun, J., Bellmann-Strobl, J., Ruprecht, K., Paul, F., Wurfel, J., Sack, I., 2016. Higher-resolution MR elastography reveals early mechanical signatures of neuroinflammation in patients with clinically isolated syndrome. J. Magn. Reson. Imaging 44, 51–58.

Freimann, F.B., Muller, S., Streitberger, K.J., Guo, J., Rot, S., Ghori, A., Vajkoczy, P., Reiter, R., Sack, I., Braun, J., 2013. MR elastography in a murine stroke model reveals correlation of macroscopic viscoelastic properties of the brain with neuronal density. NMR Biomed. 26, 1534–1539.

Freimann, F.B., Streitberger, K.J., Klatt, D., Lin, K., McLaughlin, J., Braun, J., Sprung, C., Sack, I., 2012. Alteration of brain viscoelasticity after shunt treatment in normal pressure hydrocephalus. Neuroradiology 54, 189–196.

Gennisson, J.L., Catheline, S., Chaffai, S., Fink, M., 2003. Transient elastography in anisotropic medium: application to the measurement of slow and fast shear wave speeds in muscles. J. Acoust. Soc. Am. 114, 536–541.

Gennisson, J.L., Deffieux, T., Mace, E., Montaldo, G., Fink, M., Tanter, M., 2010. Viscoelastic and anisotropic mechanical properties of in vivo muscle tissue assessed by supersonic shear imaging. Ultrasound Med. Biol. 36, 789–801.

Green, M.A., Bilston, L.E., Sinkus, R., 2008. In vivo brain viscoelastic properties measured by magnetic resonance elastography. NMR Biomed. 21, 755–764.

Guo, J., Hirsch, S., Fehlner, A., Papazoglou, S., Scheel, M., Braun, J., Sack, I., 2013. Towards an elastographic atlas of brain anatomy. PLoS One 8, e71807.

Guo, J., Posnansky, O., Hirsch, S., Scheel, M., Taupitz, M., Braun, J., Sack, I., 2012. Fractal network dimension and viscoelastic powerlaw behavior: II. An experimental study of structure-mimicking phantoms by magnetic resonance elastography. Phys. Med. Biol. 57, 4041–4053.

Hain, E.G., Klein, C., Munder, T., Braun, J., Riek, K., Mueller, S., Sack, I., Steiner, B., 2016. Dopaminergic neurodegeneration in the mouse is associated with decrease of viscoelasticity of substantia nigra tissue. PLoS One 11, e0161179.

Hatt, A., Cheng, S., Tan, K., Sinkus, R., Bilston, L.E., 2015. MR elastography can Be used to measure brain stiffness changes as a result of altered cranial venous drainage during jugular compression. AJNR Am. J. Neuroradiol. 36, 1971–1977.

Hetzer, S., Birr, P., Fehlner, A., Hirsch, S., Dittmann, F., Barnhill, E., Braun, J., Sack, I., 2017. Perfusion alters stiffness of deep gray matter. J. Cereb. Blood Flow. Metab. https://doi.org/10.1177/0271678X17691530. Epub ahead of print.

Hirsch, S., Guo, J., Reiter, R., Papazoglou, S., Kroencke, T., Braun, J., Sack, I., 2014. MR elastography of the liver and the spleen using a piezoelectric driver, single-shot wave-field acquisition, and multifrequency dual parameter reconstruction. Magn. Reson Med. 71, 267–277.

Hiscox, L.V., Johnson, C.L., Barnhill, E., McGarry, M.D., Huston, J., van Beek, E.J., Starr, J.M., Roberts, N., 2016. Magnetic resonance elastography (MRE) of the human brain: technique, findings and clinical applications. Phys. Med. Biol. 61, R401–R437.

Hoover, J.M., Morris, J.M., Meyer, F.B., 2011. Use of preoperative magnetic resonance imaging T1 and T2 sequences to determine intraoperative meningioma consistency. Surg. Neurol. Int. 2, 142.

Hughes, J.D., Fattahi, N., Van Gompel, J., Arani, A., Meyer, F., Lanzino, G., Link, M.J., Ehman, R., Huston, J., 2015. Higher-resolution magnetic resonance elastography in

meningiomas to determine intratumoral consistency. Neurosurgery 77, 653–658 discussion 658–659.
Huston 3rd, J., Murphy, M.C., Boeve, B.F., Fattahi, N., Arani, A., Glaser, K.J., Manduca, A., Jones, D.T., Ehman, R.L., 2016. Magnetic resonance elastography of frontotemporal dementia. J. Magn. Reson. Imaging 43, 474–478.
Johnson, C.L., Holtrop, J.L., McGarry, M.D., Weaver, J.B., Paulsen, K.D., Georgiadis, J.G., Sutton, B.P., 2014. 3D multislab, multishot acquisition for fast, whole-brain MR elastography with high signal-to-noise efficiency. Magn. Reson Med. 71, 477–485.
Johnson, C.L., McGarry, M.D., Gharibans, A.A., Weaver, J.B., Paulsen, K.D., Wang, H., Olivero, W.C., Sutton, B.P., Georgiadis, J.G., 2013a. Local mechanical properties of white matter structures in the human brain. Neuroimage 79, 145–152.
Johnson, C.L., McGarry, M.D., Van Houten, E.E., Weaver, J.B., Paulsen, K.D., Sutton, B.P., Georgiadis, J.G., 2013b. Magnetic resonance elastography of the brain using multishot spiral readouts with self-navigated motion correction. Magn. Reson Med. 70, 404–412.
Johnson, C.L., Schwarb, H.M.D.J.M., Anderson, A.T., Huesmann, G.R., Sutton, B.P., Cohen, N.J., 2016. Viscoelasticity of subcortical gray matter structures. Hum. Brain Mapp. 37, 4221–4233.
Juge, L., Petiet, A., Lambert, S.A., Nicole, P., Chatelin, S., Vilgrain, V., Van Beers, B.E., Bilston, L.E., Sinkus, R., 2015. Microvasculature alters the dispersion properties of shear waves–a multi-frequency MR elastography study. NMR Biomed. 28, 1763–1771.
Kashimura, H., Inoue, T., Ogasawara, K., Arai, H., Otawara, Y., Kanbara, Y., Ogawa, A., 2007. Prediction of meningioma consistency using fractional anisotropy value measured by magnetic resonance imaging. J. Neurosurg. 107, 784–787.
Kendall, B., Pullicino, P., 1979. Comparison of consistency of meningiomas and CT appearances. Neuroradiology 18, 173–176.
Klatt, D., Hamhaber, U., Asbach, P., Braun, J., Sack, I., 2007. Noninvasive assessment of the rheological behavior of human organs using multifrequency MR elastography: a study of brain and liver viscoelasticity. Phys. Med. Biol. 52, 7281–7294.
Klatt, D., Johnson, C.L., Magin, R.L., 2015. Simultaneous, multidirectional acquisition of displacement fields in magnetic resonance elastography of the in vivo human brain. J. Magn. Reson. Imaging 42, 297–304.
Klein, C., Hain, E.G., Braun, J., Riek, K., Mueller, S., Steiner, B., Sack, I., 2014. Enhanced adult neurogenesis increases brain stiffness: in vivo magnetic resonance elastography in a mouse model of dopamine depletion. PLoS One 9, e92582.
Kruse, S.A., Rose, G.H., Glaser, K.J., Manduca, A., Felmlee, J.P., Jack Jr., C.R., Ehman, R.L., 2008. Magnetic resonance elastography of the brain. Neuroimage 39, 231–237.
Kruse, S.A., Smith, J.A., Lawrence, A.J., Dresner, M.A., Manduca, A., Greenleaf, J.F., Ehman, R.L., 2000. Tissue characterization using magnetic resonance elastography: preliminary results. Phys. Med. Biol. 45, 1579–1590.
Lambert, S.A., Nasholm, S.P., Nordsletten, D., Michler, C., Juge, L., Serfaty, J.M., Bilston, L., Guzina, B., Holm, S., Sinkus, R., 2015. Bridging three orders of magnitude: multiple scattered waves sense fractal microscopic structures via dispersion. Phys. Rev. Lett. 115, 094301.
Lipp, A., Trbojevic, R., Paul, F., Fehlner, A., Hirsch, S., Scheel, M., Noack, C., Braun, J., Sack, I., 2013. Cerebral magnetic resonance elastography in supranuclear palsy and idiopathic Parkinson's disease. Neuroimage Clin. 3, 381–387.
McGarry, M.D.J., Van Houten, E.E.W., Johnson, C.L., Georgiadis, J.G., Sutton, B.P., Weaver, J.B., Paulsen, K.D., 2012. Multiresolution MR elastography using nonlinear inversion. Med. Phys. 39, 6388–6396.
Millward, J.M., Guo, J., Berndt, D., Braun, J., Sack, I., Infante-Duarte, C., 2015. Tissue structure and inflammatory processes shape viscoelastic properties of the mouse brain. NMR Biomed. 28, 831–839.
Munder, T., Pfeffer, A., Schreyer, S., Guo, J., Braun, J., Sack, I., Steiner, B., Klein, C., 2017. MR elastography detection of early viscoelastic response of the murine hippocampus to amyloid beta accumulation and neuronal cell loss due to Alzheimer's disease. J. Magn. Reson. Imaging. https://doi.org/10.1002/jmri.25741. Epub ahead of print.
Murphy, M.C., Curran, G.L., Glaser, K.J., Rossman, P.J., Huston 3rd, J., Poduslo, J.F., Jack Jr., C.R., Felmlee, J.P., Ehman, R.L., 2012. Magnetic resonance elastography of the brain in a mouse model of Alzheimer's disease: initial results. Magn. Reson. Imaging 30, 535–539.
Murphy, M.C., Huston 3rd, J., Glaser, K.J., Manduca, A., Meyer, F.B., Lanzino, G., Morris, J.M., Felmlee, J.P., Ehman, R.L., 2013a. Preoperative assessment of meningioma stiffness using magnetic resonance elastography. J. Neurosurg. 118, 643–648.
Murphy, M.C., Huston 3rd, J., Jack Jr., C.R., Glaser, K.J., Manduca, A., Felmlee, J.P., Ehman, R.L., 2011. Decreased brain stiffness in Alzheimer's disease determined by magnetic resonance elastography. J. Magn. Reson. Imaging 34, 494–498.
Murphy, M.C., Huston 3rd, J., Jack Jr., C.R., Glaser, K.J., Senjem, M.L., Chen, J., Manduca, A., Felmlee, J.P., Ehman, R.L., 2013b. Measuring the characteristic topography of brain stiffness with magnetic resonance elastography. PLoS One 8, e81668.
Murphy, M.C., Jones, D.T., Jack Jr., C.R., Glaser, K.J., Senjem, M.L., Manduca, A., Felmlee, J.P., Carter, R.E., Ehman, R.L., Huston 3rd, J., 2016. Regional brain stiffness changes across the Alzheimer's disease spectrum. Neuroimage Clin. 10, 283–290.
Muthupillai, R., Lomas, D.J., Rossman, P.J., Greenleaf, J.F., Manduca, A., Ehman, R.L., 1995. Magnetic resonance elastography by direct visualization of propagating acoustic shear waves. Science 269, 1854–1857.
Oliphant, T.E., Manduca, A., Ehman, R.L., Greenleaf, J.F., 2001. Complex-valued stiffness reconstruction for magnetic resonance elastography by algebraic inversion of the differential equation. Magn. Reson Med. 45, 299–310.
Papazoglou, S., Hamhaber, U., Braun, J., Sack, I., 2008. Algebraic Helmholtz inversion in planar magnetic resonance elastography. Phys. Med. Biol. 53, 3147–3158.
Papazoglou, S., Rump, J., Braun, J., Sack, I., 2006. Shear wave group velocity inversion in MR elastography of human skeletal muscle. Magn. Reson Med. 56, 489–497.
Perry, A., Graffeo, C.S., Fattahi, N., ElSheikh, M.M., Cray, N., Arani, A., Ehman, R.L., Glaser, K.J., Manduca, A., Meyer, F.B., Huston 3rd, J., 2017. Clinical correlation of abnormal findings on magnetic resonance elastography in idiopathic normal pressure hydrocephalus. World Neurosurg. 99, 695–700 e691.
Posnansky, O., Guo, J., Hirsch, S., Papazoglou, S., Braun, J., Sack, I., 2012. Fractal network dimension and viscoelastic powerlaw behavior: I. A modeling approach based on a coarse-graining procedure combined with shear oscillatory rheometry. Phys. Med. Biol. 57, 4023–4040.
Riek, K., Millward, J.M., Hamann, I., Mueller, S., Pfueller, C.F., Paul, F., Braun, J., Infante-Duarte, C., Sack, I., 2012. Magnetic resonance elastography reveals altered brain viscoelasticity in experimental autoimmune encephalomyelitis. Neuroimage Clin. 1, 81–90.
Romano, A., Guo, J., Prokscha, T., Meyer, T., Hirsch, S., Braun, J., Sack, I., Scheel, M., 2014. In vivo waveguide elastography: effects of neurodegeneration in patients with amyotrophic lateral sclerosis. Magn. Reson Med. 72, 1755–1761.
Romano, A., Scheel, M., Hirsch, S., Braun, J., Sack, I., 2012. In vivo waveguide elastography of white matter tracts in the human brain. Magn. Reson Med. 68, 1410–1422.
Sack, I., Beierbach, B., Wuerfel, J., Klatt, D., Hamhaber, U., Papazoglou, S., Martus, P., Braun, J., 2009. The impact of aging and gender on brain viscoelasticity. Neuroimage 46, 652–657.
Sack, I., Streitberger, K.J., Krefting, D., Paul, F., Braun, J., 2011. The influence of physiological aging and atrophy on brain viscoelastic properties in humans. PLoS One 6, e23451.
Schmidt, J.L., Tweten, D.J., Benegal, A.N., Walker, C.H., Portnoi, T.E., Okamoto, R.J., Garbow, J.R., Bayly, P.V., 2016. Magnetic resonance elastography of slow and fast shear waves illuminates differences in shear and tensile moduli in anisotropic tissue. J. Biomech. 49, 1042–1049.
Schregel, K., Wuerfel, E., Garteiser, P., Gemeinhardt, I., Prozorovski, T., Aktas, O., Merz, H., Petersen, D., Wuerfel, J., Sinkus, R., 2012. Demyelination reduces brain parenchymal stiffness quantified in vivo by magnetic resonance elastography. Proc. Natl. Acad. Sci. U. S. A. 109, 6650–6655.
Schwarb, H., Johnson, C.L., Daugherty, A.M., Hillman, C.H., Kramer, A.F., Cohen, N.J., Barbey, A.K., 2017. Aerobic fitness, hippocampal viscoelasticity, and relational memory performance. Neuroimage 153, 179–188.
Schwarb, H., Johnson, C.L., McGarry, M.D., Cohen, N.J., 2016. Medial temporal lobe viscoelasticity and relational memory performance. Neuroimage 132, 534–541.
Smith, K.A., Leever, J.D., Hylton, P.D., Camarata, P.J., Chamoun, R.B., 2016. Meningioma consistency prediction utilizing tumor to cerebellar peduncle intensity on T2-weighted magnetic resonance imaging sequences: TCTI ratio. J. Neurosurg. 1–7.
Streitberger, K.J., Sack, I., Krefting, D., Pfuller, C., Braun, J., Paul, F., Wuerfel, J., 2012. Brain viscoelasticity alteration in chronic-progressive multiple sclerosis. PLoS One 7, e29888.
Streitberger, K.J., Wiener, E., Hoffmann, J., Freimann, F.B., Klatt, D., Braun, J., Lin, K., McLaughlin, J., Sprung, C., Klingebiel, R., Sack, I., 2011. In vivo viscoelastic properties of the brain in normal pressure hydrocephalus. NMR Biomed. 24, 385–392.
Suzuki, Y., Sugimoto, T., Shibuya, M., Sugita, K., Patel, S.J., 1994. Meningiomas: correlation between MRI characteristics and operative findings including consistency. Acta Neurochir. (Wien) 129, 39–46.
Tweten, D.J., Okamoto, R.J., Bayly, P.V., 2017. Requirements for accurate estimation of anisotropic material parameters by magnetic resonance elastography: a computational study. Magn. Reson Med. https://doi.org/10.1002/mrm.26600. Epub ahead of print.
Tweten, D.J., Okamoto, R.J., Schmidt, J.L., Garbow, J.R., Bayly, P.V., 2015. Estimation of material parameters from slow and fast shear waves in an incompressible, transversely isotropic material. J. Biomech. 48, 4002–4009.
Van Houten, E.E., Miga, M.I., Weaver, J.B., Kennedy, F.E., Paulsen, K.D., 2001. Three-dimensional subzone-based reconstruction algorithm for MR elastography. Magn. Reson Med. 45, 827–837.
Van Houten, E.E., Paulsen, K.D., Miga, M.I., Kennedy, F.E., Weaver, J.B., 1999. An overlapping subzone technique for MR-based elastic property reconstruction. Magn. Reson Med. 42, 779–786.
Wuerfel, J., Paul, F., Beierbach, B., Hamhaber, U., Klatt, D., Papazoglou, S., Zipp, F., Martus, P., Braun, J., Sack, I., 2010. MR-elastography reveals degradation of tissue integrity in multiple sclerosis. Neuroimage 49, 2520–2525.
Xu, L., Lin, Y., Han, J.C., Xi, J.N., Shen, H., Gao, P.Y., 2007. Magnetic resonance elastography of brain tumors: preliminary results. Acta Radiol. 48, 327–330.
Yamaguchi, N., Kawase, T., Sagoh, M., Ohira, T., Shiga, H., Toya, S., 1997. Prediction of consistency of meningiomas with preoperative magnetic resonance imaging. Surg. Neurol. 48, 579–583.
Yin, Z., Glaser, K.J., Manduca, A., Van Gompel, J.J., Link, M.J., Hughes, J.D., Romano, A., Ehman, R.L., Huston 3rd, J., 2015. Slip interface imaging predicts tumor-brain adhesion in vestibular schwannomas. Radiology 277, 507–517.
Yin, Z., Hughes, J.D., Glaser, K.J., Manduca, A., Van Gompel, J., Link, M.J., Romano, A., Ehman, R.L., Huston 3rd, J., 2017. Slip interface imaging based on MR-elastography preoperatively predicts meningioma-brain adhesion. J. Magn. Reson. Imaging 46 (4), 1007–1016.
Zhang, J., Green, M.A., Sinkus, R., Bilston, L.E., 2011. Viscoelastic properties of human cerebellum using magnetic resonance elastography. J. Biomech. 44, 1909–1913.